Energy & Environmental Science

PAPER

View Article Online
View Journal | View Issue

Cite this: *Energy Environ. Sci.*, 2015, **8**, 2480

Carbon capture turned upside down: high-temperature adsorption & low-temperature desorption (HALD)†

Lennart Joos,[a] Kurt Lejaeghere,[a] Johanna M. Huck,[b] Veronique Van Speybroeck[a] and Berend Smit*[bcd]

Received 30th May 2015,
Accepted 30th June 2015

DOI: 10.1039/c5ee01690h

www.rsc.org/ees

Carbon capture & sequestration (CCS) could reduce CO_2 emissions from large fossil-fuel power plants on the short term, but the high energy penalty of the process hinders its industrial deployment. Moreover, the utility of nanoporous materials, known to be selective for the CO_2/N_2 separation, is drastically reduced due to the competitive adsorption with H_2O. Taking advantage of the power plant's waste heat to perform CCS while at the same time surmounting the negative effect of H_2O is therefore an attractive idea. We propose an upside-down approach for CCS in nanoporous materials, high-temperature adsorption & low-temperature desorption (HALD), that exploits the temperature-dependent competitive adsorption of CO_2 and H_2O. First, we provide a theoretical background for this entropy-driven behavior and demonstrate under what conditions competitive adsorption can be in favor of CO_2 at high temperature and in favor of H_2O at low temperature. Then, molecular simulations in all-silica MFI provide a proof of concept. The International Zeolite Association database is subsequently screened for potential candidates and finally, the most promising materials are selected using a post-Pareto search algorithm. The proposed post-Pareto approach is able to select the material that shows an optimal combination of multiple criteria, such as CO_2/H_2O selectivity, CO_2/N_2 selectivity, CO_2 uptake and H_2O uptake. As a conclusion, this work provides new perspectives to reduce the energy requirement for CCS and to overcome the competitive adsorption of H_2O.

Broader context

Utilizing the residual heat of a power plant's flue gas to capture the CO_2 from this $CO_2/N_2/H_2O$ mixture could drastically reduce the energy requirement of carbon capture and sequestration (CCS). The novel approach to CCS presented here, high-temperature adsorption & low-temperature desorption (HALD) of CO_2 in zeolites, exploits the temperature-dependent competitive adsorption of CO_2 and H_2O. A theoretical model demonstrates that differences in the adsorption enthalpy and entropy for CO_2 and H_2O can favor CO_2 adsorption at high temperature and H_2O uptake at low temperature. Using Grand Canonical Monte Carlo simulations, we perform a screening of the existing zeolite topologies to assess their adsorption properties. Afterwards, a post-Pareto analysis identifies the most promising materials. The proposed HALD behavior can be used in a temperature-swing process, which would not require the input of energy for regeneration, but instead would recover the CO_2 by saturating the material with water. In addition, the deeper understanding of the entropy-driven competitive adsorption of CO_2 and H_2O opens new perspectives to overcome the detrimental effect of water.

1 Introduction

Nearly half of the world's CO_2 emissions originate from fossil-fuel power plants. Cutting emissions at these concentrated CO_2 sources would therefore be very effective in fighting climate change.[1–4] Carbon capture & sequestration (CCS) is one of the most promising technologies to reduce the CO_2 emissions from large power plants on the short term. CCS can act as an intermediary measure in the transition from fossil fuels to renewable energy, tackling CO_2 emissions of the fossil fuel era, while providing breathing room for renewable technologies to be developed. There are nanoporous materials that can adsorb

[a] *Center for Molecular Modeling, Ghent University, B-9052 Zwijnaarde, Belgium. E-mail: veronique.vanspeybroeck@ugent.be*
[b] *Department of Chemical and Biomolecular Engineering, University of California, Berkeley, Berkeley, CA 94720-1462, USA. E-mail: Berend-Smit@berkeley.edu*
[c] *Department of Chemistry, University of California, Berkeley, Berkeley, CA 94720-1462, USA*
[d] *Laboratory of Molecular Simulation, Institut des Sciences et Ingénierie Chimiques, Valais, Rue d'Industrie 17, Ecole Polytechnique Fédérale de Lausanne (EPFL), CH-1951 Sion, Switzerland*

† Electronic supplementary information (ESI) available: Calculation of entropy, details of the force field, influence of cations and sensitivity of the Pareto analysis. See DOI: 10.1039/c5ee01690h

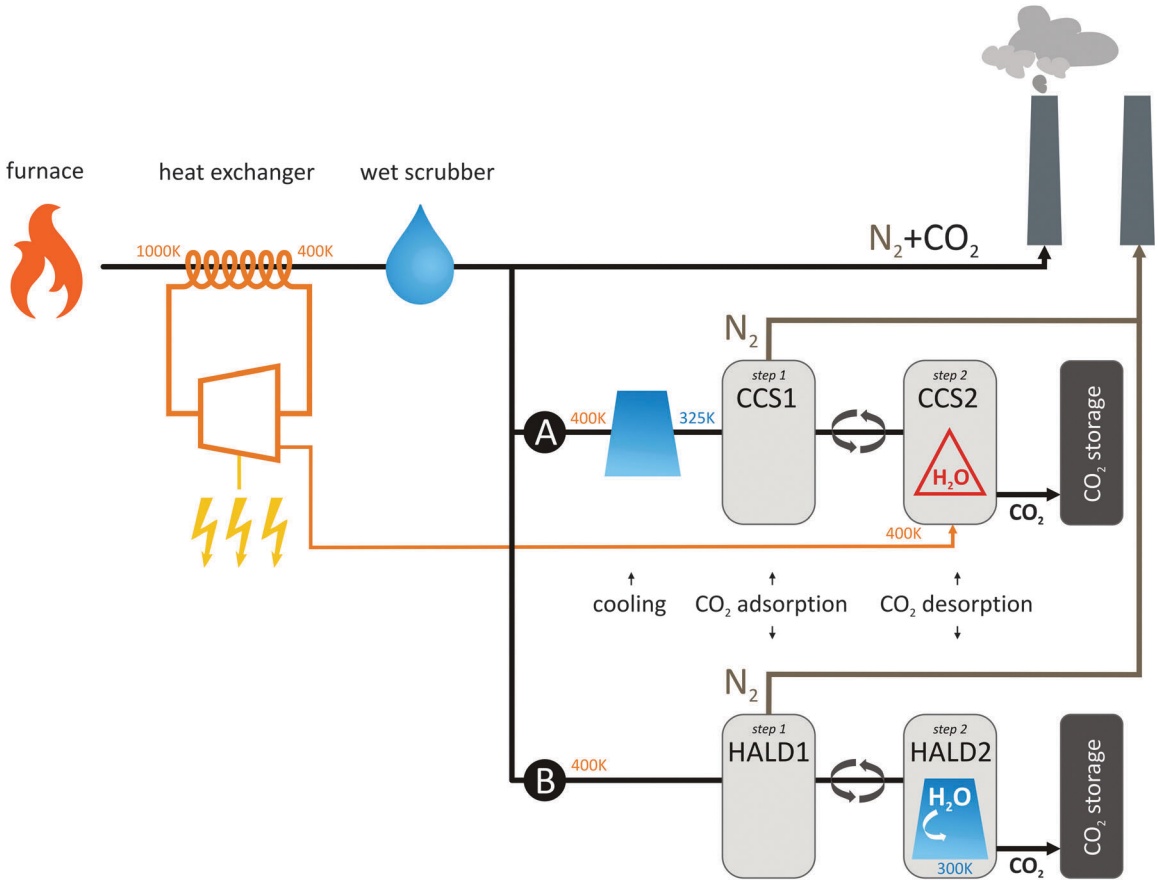

Fig. 1 Layout of a fossil fuel-fired power plant. In the heat exchanger, high-pressure stream is produced around 400 K, which is used to drive a turbine and generate electricity. NO_x and SO_x molecules are removed in a wet scrubber and the exhaust gases are typically released into the atmosphere with residual heat at 400 K, because the valorization of low-temperature heat is difficult and the condensation of H_2O undesired. (A) Represents a power plant retrofitted with conventional carbon capture technology based on CO_2 adsorption on a nanoporous material. The exhaust gases are first cooled and CO_2 is subsequently adsorbed. Regeneration of the bed requires a parasitic energy from the power plant (orange arrow), which is even higher when H_2O is present (H_2O warning sign). (B) is a power plant retrofitted with the proposed high-temperature adsorption, low-temperature desorption technology. The regeneration step comprises cooling and saturating the material with H_2O.

CO_2 and separate it from N_2, but the high energy penalty and associated monetary cost CCS imposes on the plant present a serious bottleneck for its industrial deployment. Moreover, most materials show a significant performance drop when H_2O is present in the exhaust stream, further increasing the energy penalty for CCS and hampering its large-scale application.

In Fig. 1, a typical fossil-fuel power plant is outlined schematically. A fossil fuel is burned and the hot combustion gases are brought into contact with a heat exchanger. The high-pressure steam that is produced drives a turbine, which subsequently produces electricity. The exhaust gases still contain some residual heat (around 400 K), but it is difficult to convert into work or electricity and therefore essentially waste heat. In many countries, environmental regulations stipulate that the most hazardous components should be removed from the flue gases before they are released into the atmosphere. Therefore, components such as NO_x and SO_x are removed in 'wet scrubbers',[5] where flue gases are contacted with a reactive solution that removes the undesired components from the gas stream. As the hot gases go through an aqueous solution, some H_2O evaporates from the scrubber into the exhaust gases. In order to avoid corrosion in downstream equipment, it is important that this water does not condense, so the exhaust gases should leave the stacks of the power plant well above the saturation point of H_2O.

To remove CO_2 from the exhaust gases of an existing power plant, a post-combustion carbon capture facility could be installed before the flue gases leave the stacks. Currently, the most mature technology to selectively capture CO_2 from post-combustion flue gases is amine scrubbing.[6,7] The flue gases are washed with an amine solution, in which CO_2 binds with the amines in a chemical reaction. The solution is regenerated in a second step by 'stripping' the CO_2 from the amines at high temperature.

Heating the dilute aqueous mixture imposes a severe energy penalty on the process and alternative technologies have therefore been explored. Several nanoporous materials demonstrated a high CO_2/N_2 selectivity, a good CO_2 uptake as well as a less energy demanding regeneration than the amine solutions.[8,9] Advantageous materials can be found among zeolites,[10,11] cation-exchanged zeolites (CEZ),[12,13] metal–organic frameworks

(MOFs),[14,15] zeolitic imidazolate frameworks (ZIFs)[16,17] and porous polymer networks (PPNs).[18,19]

In the current work, we focus on zeolites. Zeolites are nanoporous materials that are mainly built from SiO_2, although their frameworks may also contain Al, Ge, P and some other elements.[20] From the thousands of theoretically possible topologies only 225 framework topologies have actually been synthesized and are included in the database of the international zeolite association (IZA).[21] Due to its industrial availability as well as commercial applications, all-silica MFI (also known as silicalite-1) is often used as a reference material.[22–30]

Fig. 1(A) and 2(A) show how an existing power plant can be retrofitted with CCS technology based on nanoporous materials. CCS is a cyclic two step process: in step 1, the flue gas is sent over a bed of the nanoporous material, which retains CO_2 while letting N_2 go through towards the stacks. The CO_2 uptake and CO_2/N_2 selectivity of nanoporous materials drop significantly with temperature, so the incoming stream is cooled, typically to 325 K. In step 2, the CO_2 saturated bed is taken out of the exhaust gases and regenerated by heating, applying a vacuum or both.[31,32] Either way, an energy penalty is imposed on the process, lowering the power output of the plant, which is indicated with the orange arrow in Fig. 1(A).

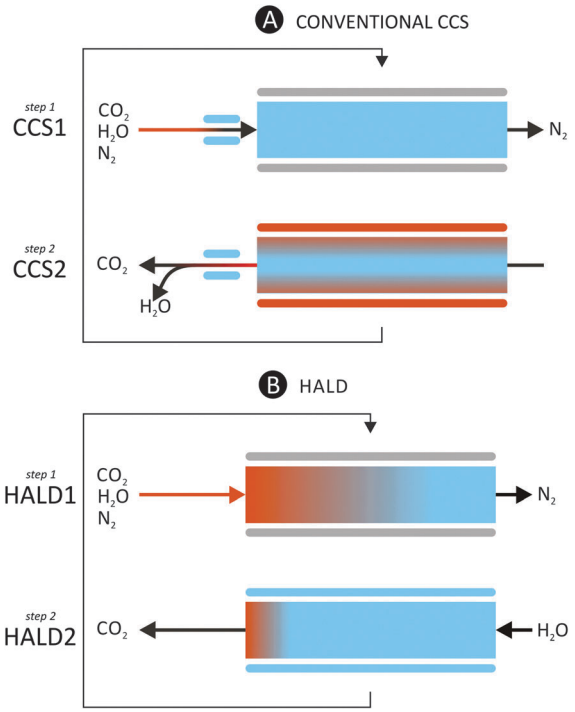

Fig. 2 (A) Conventional carbon capture based on nanoporous materials. CCS1: the exhaust gases are first cooled, CO_2 is adsorbed on a bed of a nanoporous material while N_2 is not retained. CCS2: the bed is regenerated by heating, with the presence of H_2O imposing an additional energy penalty. (B) High-temperature adsorption, low-temperature desorption (HALD). HALD1: adsorption is performed at high temperature, to favor the competition of CO_2 over H_2O, no cooling is required. HALD2: regeneration of the bed by cooling (competitive advantage of H_2O over CO_2) and saturation with H_2O.

The CCS performance of nanoporous materials can easily be evaluated with one straightforward metric: the parasitic energy, *i.e.* the energy output parasitized by CCS.[32] Although the parasitic energy of some nanoporous materials is lower than for amine scrubbing, still some 20–30% of the power plant's energy output would be used for CCS, corresponding to \$40–\$60 per tonne of CO_2 abated.[33] Additionally, H_2O in the exhaust stream has a detrimental effect on the performance of most nanoporous materials that have been proposed for CCS in the past, because most of the adsorption sites for CO_2 are fully saturated with H_2O instead. This lowers the CO_2 uptake and increases the energy for the regeneration, as H_2O also has to be removed from the adsorption bed, resulting in an even higher parasitic energy altogether. The detrimental effect of water is indicated with the H_2O warning sign in Fig. 1(A).

In this paper, we propose an alternative operation of the carbon capture process that circumvents the high energy penalty for the CO_2/N_2 separation in the presence of H_2O. CO_2 adsorption is performed at high temperature (400 K), whereas the release of CO_2 happens at low temperature, through saturation of the absorbent with H_2O. Inspiration for the proposed methodology was found in the chemisorption of NO_x on phosphotungstic acid.[34,35] At high temperature, NO_x molecules are chemisorbed in the crystal structure of the acid, substituting the H_2O molecules that were present in the crystal structure before. The NO_x moieties are released only at low temperature and in the presence of H_2O. The phenomenon of competitive adsorption of H_2O and NO_x is driven by the entropy difference between the adsorbed and desorbed molecules. Although the search for efficient absorbents is most often based on differences in adsorption enthalpy,[36,37] this and other examples show the potential of entropy-driven adsorption/desorption processes.[38,39] In HALD, we also want to exploit the entropy as a driver for competitive adsorption and desorption of CO_2 and H_2O.

A practical setup for this HALD approach is shown in Fig. 1(B) and 2(B). The carbon capture unit is installed immediately after the wet scrubbers, taking in the wet flue gas without cooling at 400 K (step 1). In step 2, the regeneration cycle, the bed is cooled down and saturated with H_2O. When the regenerated bed, empty of CO_2 but full of H_2O, is brought into contact with the hot exhaust gases again, the waste heat of the exhaust gases is used to desorb the H_2O and give CO_2 again a competitive advantage. H_2O is in this process no longer sabotaging the process, but assisting in the adsorption/desorption cycles.

In this process, CO_2/H_2O selectivity, CO_2/N_2 selectivity, CO_2 uptake and H_2O loading are important criteria. When screening a large set of materials, it is interesting to select those that perform best for the four parameters. This multicriteria selection problem can be tackled with a so-called Pareto-approach. First, the materials that outperform all other materials for at least one criterium are selected, thereby drastically reducing the number of candidates. Afterwards, a post-Pareto procedure can rank the materials in the Pareto set by determining how much one or more criteria can be improved with a minimal deterioration in all other parameters.[40] The concept of Pareto efficiency is borrowed from economics, where Pareto efficiency

indicates that resources are allocated in a way that no individual can improve his/her situation without making other individuals worse off.[41]

In this manuscript, the concept of 'high-temperature adsorption & low-temperature desorption' (HALD) is proposed. First, a Langmuir model shows how this counterintuitive approach is based on the temperature dependence of the competitive adsorption between CO_2 and H_2O. Molecular simulations on the all-silica MFI zeolite subsequently provide a proof of principle for HALD. Furthermore, the Langmuir model is tested by screening the IZA database for the expected trends and the best performing materials are selected using a post-Pareto approach. Finally, we provide an outlook on the commercialization of this technology, and the opportunities and challenges ahead.

2 Theoretical origin of HALD

The concept of high-temperature adsorption & low-temperature desorption (HALD) is based on a competitive adsorption between CO_2 and H_2O. We want to exploit a behavior in which CO_2 wins the competition at high temperatures, whereas H_2O adsorption is favored at low temperature. To introduce the concept properly, we first give a theoretical rationalization of the effects governing the process.

Fig. 3 explains the HALD approach with a breakdown of the Gibbs free adsorption energy for CO_2 and H_2O into an enthalpic and an entropic contribution, at low temperature (here chosen to be 300 K) and high temperature (here set to 400 K). The energy diagram shows a hypothetical situation where the enthalpy and entropy are assumed to be temperature-independent. In the ESI,† we justify this choice by pointing out that ΔH_{ads} and ΔS_{ads} only have a weak temperature dependence in the 300–400 K interval. For H_2O to adsorb preferentially at low temperature (and in the limit at 0 K), the adsorption enthalpy for H_2O should be more negative than for CO_2 ($\Delta H_{ads,H_2O} < \Delta H_{ads,CO_2} < 0$). If then the entropy loss upon adsorption of H_2O is higher than that of CO_2 ($\Delta S_{ads,H_2O} < \Delta S_{ads,CO_2} < 0$), there will be a temperature at which the relative order of the Gibbs free adsorption energy switches. It should also be mentioned that at high temperature,

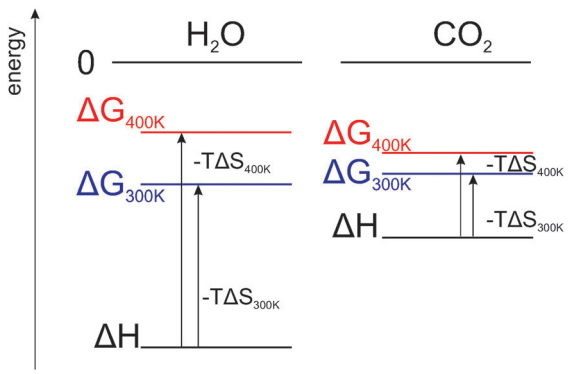

Fig. 3 Illustration of the HALD concept with a hypothetical breakdown of the Gibbs free adsorption energy for H_2O and CO_2 in an enthalpic and an entropic contribution. ΔH and ΔS are assumed temperature-independent.

the driving force for adsorption of both gas molecules has decreased significantly, as ΔG has become less negative for both gases.

A more detailed approach to the competitive adsorption of CO_2 and H_2O is to consider a Langmuir model. Assuming that both gases are competing for the same adsorption sites, the coverage of CO_2 and H_2O can be written as:

$$\theta_{CO_2} = \frac{K_{CO_2} p_{CO_2}}{1 + K_{CO_2} p_{CO_2} + K_{H_2O} p_{H_2O}} \quad (1)$$

$$\theta_{H_2O} = \frac{K_{H_2O} p_{H_2O}}{1 + K_{CO_2} p_{CO_2} + K_{H_2O} p_{H_2O}} \quad (2)$$

θ_x is the fraction of adsorption sites covered with molecule x, p_x is the partial pressure of molecule x in the gas phase and K_x is the equilibrium constant of the adsorption of molecule x. Dividing eqn (1) by 2 yields

$$\alpha = \frac{\theta_{CO_2}}{\theta_{H_2O}} = \frac{K_{CO_2} p_{CO_2}}{K_{H_2O} p_{H_2O}} \quad (3)$$

And given that

$$K_x = \exp\left(-\frac{\Delta G_{ads,x}}{RT}\right) \quad (4)$$

we can write

$$\alpha = \frac{\theta_{CO_2}}{\theta_{H_2O}} = \frac{p_{CO_2}}{p_{H_2O}} \exp\left(-\frac{\Delta G_{ads,CO_2} - \Delta G_{ads,H_2O}}{RT}\right) \quad (5)$$

or

$$\alpha = \frac{\theta_{CO_2}}{\theta_{H_2O}} = \frac{p_{CO_2}}{p_{H_2O}} \exp\left(-\frac{\Delta H_{ads,CO_2} - \Delta H_{ads,H_2O}}{RT}\right) \times \exp\left(\frac{\Delta S_{ads,CO_2} - \Delta S_{ads,H_2O}}{R}\right) \quad (6)$$

ΔG_{ads}, ΔH_{ads} and ΔS_{ads} are the Gibbs free energy, the enthalpy and the entropy of adsorption respectively, T is the temperature and R is the universal gas constant. Eqn (6) contains three terms: the first term, the ratio of the CO_2 and H_2O partial pressures, is imposed by the flue gas composition and set to be 14 kPa CO_2 and 6 kPa H_2O. That is the typical composition of the exhaust gases of coal-fired power plants, where most of the H_2O enters the exhaust gas stream during the wet scrubbing stages.[42] The second term in eqn (6) is dependent on the difference in adsorption enthalpy between CO_2 and H_2O. Finally, the third term of eqn (6) includes the difference in adsorption entropy between CO_2 and H_2O, which is expressed as a function of temperature $(\Delta S_{ads,CO_2} - \Delta S_{ads,H_2O})(T)$. In ESI,† we compare several models for assessing the adsorption entropy and we selected the model that shows the best agreement with simulation results. Overall, α (the CO_2/H_2O selectivity) can be written as a function of $\Delta H = \Delta H_{ads,CO_2} - \Delta H_{ads,H_2O}$ (the difference in adsorption enthalpy between CO_2 and H_2O, a material property) and T (the temperature, a process condition),

$$\alpha = \alpha(\Delta H, T) \quad (7)$$

Assuming that the entropic term in eqn (6) is temperature-independent, the Langmuir model implies that α increases with

increasing temperature only if $\Delta H_{CO_2} - \Delta H_{H_2O} > 0$, in line with the observations from Fig. 3. However, as the adsorption entropy $S(T)$ is dependent on temperature, the threshold from HALD to non-HALD behavior will be shifted to a slightly different value than $\Delta H_{CO_2} - \Delta H_{H_2O} = 0$. This dependence on temperature is clearly visible in Fig. 4a, which shows α_{CO_2/H_2O} as a function of ΔH for different T and Fig. 4b displays the difference between the curves at different temperatures.

In Fig. 4a, it is clear that if ΔH_{CO_2} is becoming more negative than ΔH_{H_2O}, the selectivity towards CO_2 adsorption increases for all temperatures. However, when considering the difference in selectivity at various temperatures ($\Delta\alpha$ in Fig. 4b), it becomes apparent that the CO_2/H_2O selectivity is higher at 400 K than at 300 K only if ΔH is higher than approximately -2 kJ mol^{-1}. The exact threshold value between HALD and non-HALD behavior is based on the temperature dependence of the entropy, which is determined by the model for the entropy (*cf.* ESI†) as well as by the temperatures at which the adsorption and desorption are considered. In the case of Fig. 4, if ΔH is higher than -2 kJ mol^{-1}, the selectivity for CO_2 is higher at 400 K than at 300 K and HALD is possible, whereas if ΔH is smaller than -2 kJ mol^{-1}, the selectivity towards CO_2 only decreases as a function of temperature.

Moreover, the spacing between the curves at different temperatures is highest around $\Delta H = +2$ kJ mol^{-1}, so the model predicts materials in this region show good performance for HALD. At high ΔH, the selectivity is less dependent on temperature and the corresponding materials will likely not perform well for HALD. The relatively small range between -2 kJ mol^{-1} and $+2$ kJ mol^{-1} is an indication that the method will be sensitive to small variations, in material properties (ΔH) and process conditions (T) alike.

These simple theoretical considerations give a preliminary insight into the factors that control the HALD concept. For materials with $\Delta H_{CO_2} - \Delta H_{H_2O}$ larger than -2 kJ mol^{-1}, an entropy-driven adsorption/desorption of CO_2 and H_2O is theoretically possible. We validate this concept by means of molecular simulations (Sections 4 and 5), but we first present the used methodology (Section 3).

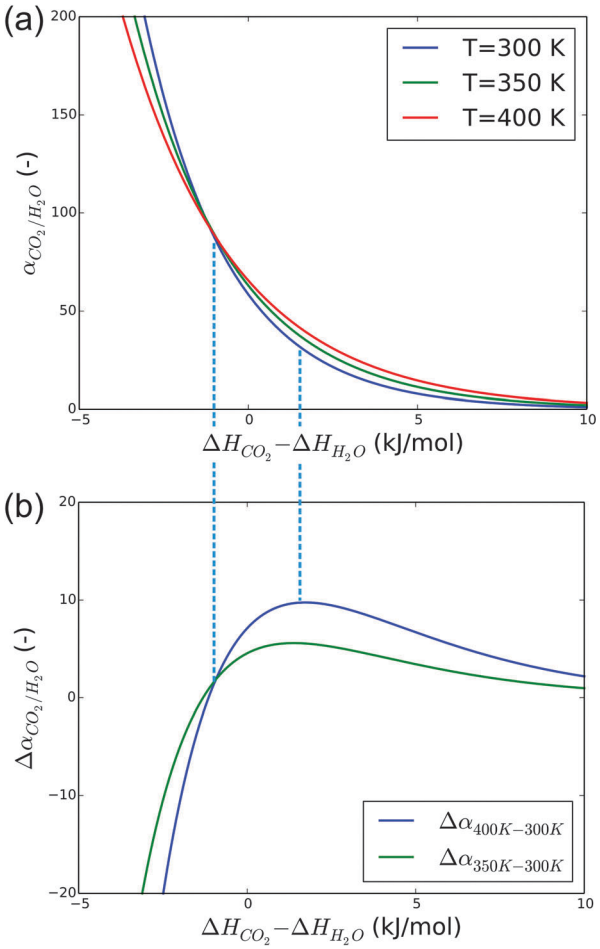

Fig. 4 (a) The CO_2/H_2O selectivity α as a function of the difference in enthalpy of adsorption of CO_2 and H_2O, $\Delta H_{CO_2} - \Delta H_{H_2O}$ for 300 K, 350 K and 400 K (b) the difference in selectivity $\Delta\alpha$ between the curves at different temperatures. The two connecting lines highlight that the curves cross around -2 kJ mol^{-1} and that the difference between the curves is maximal around +2 kJ mol^{-1}.

3 Methodology

In the previous section, we have provided a theoretical background for HALD. In the next sections, we want to validate this model with Monte Carlo simulations.[43] To do so, we need to assess the adsorption enthalpies, ΔH_{CO_2} and ΔH_{H_2O}, and the CO_2/H_2O selectivity. The adsorption enthalpies can be determined with single-component *NVT* simulations whereas the CO_2/H_2O selectivity requires grand canonical Monte Carlo (GCMC) simulations of binary mixtures. We fixed the composition of the adsorbing binary mixture at 14 kPa CO_2 and 6 kPa H_2O.[42] Adsorbate molecules are allowed to make translation, rotation, swap, and regrowth moves[44,45] and the zeolite framework is assumed rigid.[30,46] The CO_2/N_2 selectivities are determined using the ideal adsorbed solution theory (IAST)[47,48] and taken from previous work.[13,32] These studies have shown that these assumptions give reasonable predictions for CO_2/N_2 binary mixtures.

The simulations in this work are performed using existing force fields. The Lennard-Jones parameters and partial atomic charges for CO_2 are taken from the Calero force field, which has proven to be successful in reproducing experimental CO_2 isotherms in zeolite frameworks.[49] Parameters for H_2O are taken from previous work where the H_2O–H_2O interactions are modeled with the SPC/E model[50] and the H_2O-framework interactions obtained by scaling the H_2O–H_2O parameters with the ratio of the CO_2–CO_2 to CO_2-framework parameters.[51] The electrostatic contribution is computed with the Ewald summation, set at a cut-off of 12.5 Å. For all simulations, inaccessible pockets in the zeolite framework are determined with Zeo++[52–54] and blocked during the simulations. The force field parameters and atomic charges are listed in the ESI.†

The performance of a H_2O/zeolite force field is highly sensitive to the H_2O model,[26] partial charges[55] as well as the crystal structure[56] and cation content[57] of the zeolites. We used

the computationally cheap three-site H_2O model, although it will likely favor H_2O–H_2O interactions and might not describe the H_2O-framework interactions accurately. However, the predicted trends should remain valid for other force fields, except for a possible shift of the H_2O isotherms to slightly different pressures and temperatures.

We will now use these Monte Carlo simulations to demonstrate the concept of HALD

1. for the showcase example of all-silica MFI. For MFI, the difference in adsorption enthalpy between CO_2 and H_2O can be determined, so the only variable left in eqn (7) is the temperature, $\alpha(T)$.

2. in a screening of the IZA database. Across the materials in the database, $\Delta H_{CO_2} - \Delta H_{H_2O}$ varies. If the adsorption conditions are fixed at 400 K and 14 kPa CO_2/6 kPa H_2O, it is possible to examine $\alpha(\Delta H)$. This screening also allows us to pinpoint the most promising materials.

4 HALD in MFI: $\alpha(T)$

First, we want to provide a proof of concept for HALD using the commercially available all-silica MFI zeolite (often referred to as silicalite-1). For MFI, we find an adsorption enthalpy for CO_2 and H_2O of -26.6 and -31.9 kJ mol^{-1} respectively. The difference in adsorption enthalpy between CO_2 and H_2O is +5.5 kJ mol^{-1}, so according to the proposed model, this material should exhibit HALD behavior. As the ΔH is now fixed for this material, the only remaining variable in eqn (7) is the temperature, α(+5.5 kJ mol^{-1},T). Using GCMC simulations, we want to assess whether the CO_2/H_2O selectivity of MFI indeed increases with increasing temperature.

Fig. 5 displays the binary CO_2 (red) and H_2O (blue) loadings as a function of the temperature. The temperature range of this

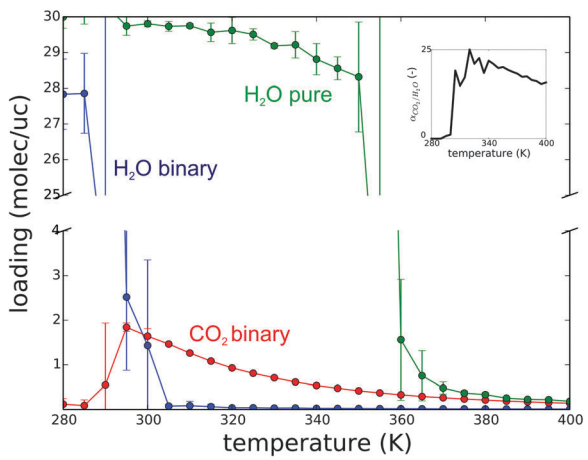

Fig. 5 Illustration of the HALD principle for MFI: the red and the blue curve represent the CO_2 and H_2O loadings as a function of the temperature when MFI is contacted with a binary mixture of 14 kPa CO_2 and 6 kPa H_2O (adsorption conditions). The green curve shows the H_2O loading in MFI equilibrated with 100 kPa pure H_2O (desorption conditions). The inset shows the CO_2/H_2O selectivity as a function of the temperature and is the ratio of the red and the blue curve.

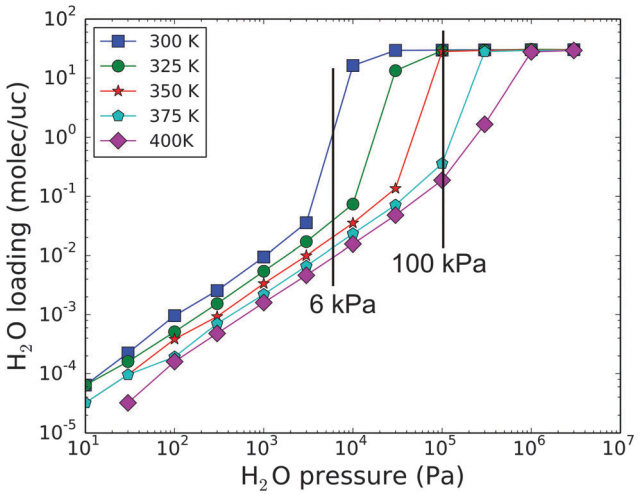

Fig. 6 Adsorption isotherms for H_2O at different temperatures. At 6 kPa, there is a drop in the loading below 325 K while at 100 kPa, this occurs between 350 and 375 K.

plot is extended towards lower temperatures, to visualize the drop in the binary H_2O loading, starting before 300 K. It is clear that the drop in the H_2O loading is more sudden than the gradual decrease in the CO_2 loading, resulting in a peak in the CO_2/H_2O selectivity. Note that at high temperatures, loadings of both components are very low (<1 molecule per unit cell). Fig. 5 also shows the H_2O loading for single-component H_2O (green) adsorption at 100 kPa. At 100 kPa and 300 K (low temperature desorption conditions in HALD), the material is fully saturated with H_2O. At higher temperatures, there is a sudden drop in the H_2O loading. The drops/steps in the H_2O loadings can also be observed in the pure H_2O isotherms in Fig. 6. For all isotherms, there is a pressure at which the H_2O suddenly increases and the framework saturates with H_2O. The step moves towards higher pressures with increasing temperature. At a fixed pressure, the same step is visible: at 100 kPa for instance, the CO_2 drops drastically between 350 and 375 K. At 6 kPa on the other hand, this drop already occurs at 300 K. The CO_2 isotherm does not displays such a sudden drop and can be seen in ESI† (Fig. S6).

The steps correspond to a sudden saturation of the framework with water as an extensive H_2O network forms. This has implications for the H_2O adsorption enthalpy (Fig. 7). At low loadings (<1 water molecule per unit cell), the adsorption enthalpy is as weak as -20 kJ mol^{-1}. Near saturation however, ΔH_{H_2O} can range from -45 to -75 kJ mol^{-1}. It is important to notice here that it is hard to uniquely define 'the' H_2O adsorption enthalpy: at too low loadings, the adsorption properties of the H_2O network are not taken into account, while at high loadings, the spread on the adsorption enthalpy is large. Moreover, the step region is poorly sampled.

To understand the origin of the discrepancy between theory and simulations, Fig. 8 shows the CO_2/H_2O selectivity as a function of the temperature. The black curve represents the data from the simulations of a binary mixture, where the CO_2/H_2O selectivity is defined as the ratio of the CO_2 and H_2O loadings.

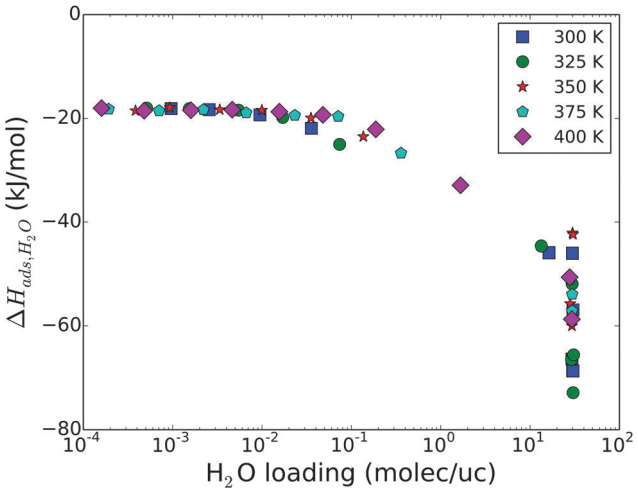

Fig. 7 Adsorption enthalpy for H_2O as a function of loading. Data were gathered from the H_2O isotherms at different temperatures.

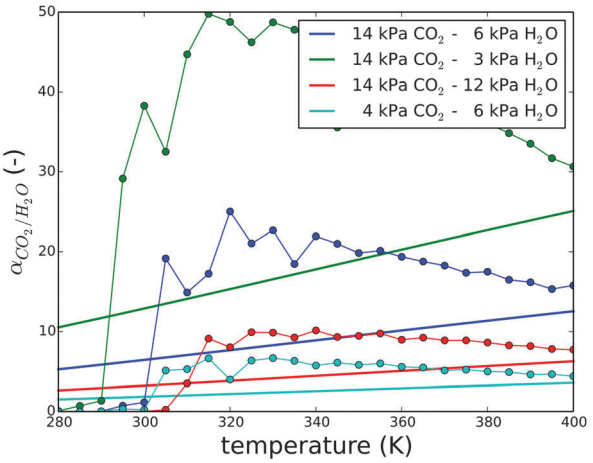

Fig. 9 Influence of the CO_2 and H_2O partial pressure in the binary mixture on the CO_2/H_2O selectivity as a function of the temperature. The solid lines represent the Langmuir model, the points are the simulation results.

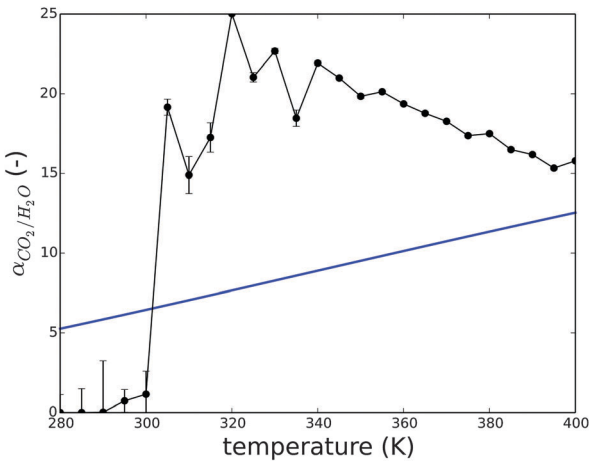

Fig. 8 The CO_2/H_2O selectivity as a function of the temperature. The black line shows the simulation results whereas the blue line represents the Langmuir model, α(+5.5 kJ mol^{-1}, T). The peak in the simulated selectivities is related to the sudden drop in the H_2O loading (blue curve in Fig. 5).

The blue curve on the other hand is the Langmuir model for MFI from eqn (6). It is clear that for both curves, the CO_2/H_2O selectivity is higher at 400 K than at 300 K. The material is therefore suitable for the HALD process. However, the monotonous rise in the theoretical $\alpha(T)$ curve is not seen in the simulation results. The peak in the simulated selectivities is related to the sudden drop in the H_2O loading (blue curve in Fig. 5), which cannot be described with the Langmuir model.

Fig. 9 demonstrates the sensitivity of the HALD method on the flue gas composition. The solid lines represent the Langmuir model from eqn (6), the connected points in the same color are taken from the simulations at the corresponding partial pressures. The blue line, corresponding to a binary mixture with 14 kPa CO_2 and 6 kPa H_2O is taken as a reference. When the H_2O partial pressure is reduced from 6 kPa to 3 kPa (green line), the Langmuir model predicts that the CO_2/H_2O selectivity to be higher. The simulations confirm this and show that the peak in the selectivity occurs at lower temperature than was the case for the reference mixture (blue line). On the other hand, when the H_2O partial pressure in the flue gas is doubled compared to the reference case, the CO_2/H_2O selectivity is lower and the peak occurs at higher temperatures. Finally, we also considered a situation where the H_2O partial pressure is kept at the original 6 kPa and the CO_2 partial pressure is decreased from 14 kPa (the flue gas composition of a coal-fired power plant) to 4 kPa (the composition of exhaust gases of a natural gas-fired power plant). In this case, the peak occurs at the same temperature as for the reference, whereas the CO_2/H_2O selectivity is lower. As a general conclusion, the CO_2/H_2O selectivity is mainly driven by the partial pressures of CO_2 and H_2O, which is clear from the first term in the Langmuir model and confirmed by the simulations. The temperature at which the peak occurs is related to the sudden H_2O desorption from the material and is imposed by the partial pressure of H_2O in the binary mixture (see Fig. 6).

Furthermore, we emphasize that adsorption at 400 K and desorption at 300 K are chosen process conditions and could be changed to optimize the HALD behavior. For instance, the CO_2/H_2O selectivity peaks at 320 K (Fig. 5), so adsorption at that temperature offers a competitive advantage for CO_2 adsorption. However, if the amount of adsorbed CO_2 is important (for instance to minimize the size of the adsorption bed), then adsorption at 310 K may become more favorable, as the CO_2 loading is still relatively high, while the step in the H_2O loading has already occurred. In Section 6, we will return to the point of simultaneously optimizing the CO_2/H_2O selectivity and CO_2 loading at high temperature.

Finally, we provide a short outlook on the possibilities of cation exchanged zeolites (CEZs). Extra-framework cations balance the net negative charge, which is introduced when some silicon atoms in the framework are replaced by aluminum atoms. In Fig. 10, the CO_2/H_2O selectivity is shown as a function of the temperature for different Si/Al ratios in the MFI framework

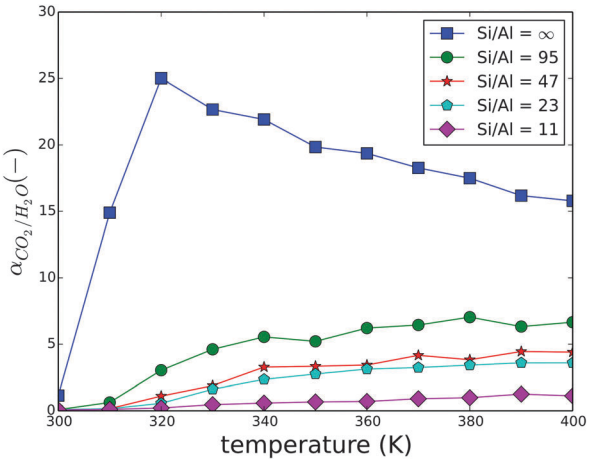

Fig. 10 CO_2/H_2O selectivity as a function of the temperature, for different Si/Al ratios in the MFI framework. The net negative charge introduced by aluminum is countered by Na^+ cations.

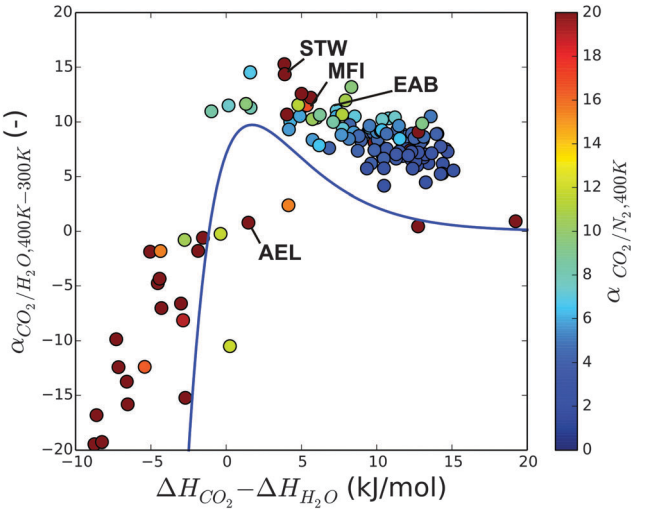

Fig. 11 Difference between the CO_2/H_2O selectivity α_{CO_2/H_2O}, at 400 K and 300 K as a function of the difference in adsorption enthalpy between H_2O and CO_2, $\Delta H_{CO_2} - \Delta H_{H_2O}$, color coded with the CO_2/N_2 selectivity at 400 K. The solid blue line indicates the behavior as predicted by the Langmuir model.

and with Na^+ countercations. CEZs have lower CO_2/H_2O selectivities than the all-silica framework, with a decreasing selectivity as the Si/Al ratio becomes lower. For all finite Si/Al ratios considered moreover, the peak in the CO_2/H_2O selectivity of the all-silica MFI framework (Si/Al = ∞) disappears and the increase in selectivity is monotonous as a function of temperature. Indeed, the extra-framework Na^+ cations are easily coordinated with H_2O, decreasing the hydrophobicity of the zeolite and increasing the competitive advantage of H_2O.

In conclusion, it is theoretically possible to exploit the competitive adsorption of CO_2 and H_2O for HALD in MFI. The HALD principle is applicable in a wide range of CO_2 and H_2O partial pressures and was also demonstrated for CEZs.

5 IZA database screening: $\alpha(\Delta H)$

MFI provides a promising proof of principle for the HALD concept. Now, we want to identify the most interesting materials for HALD from the IZA database of all-silica zeolites.[21] Across the different zeolites, $\Delta H_{CO_2} - \Delta H_{H_2O}$ varies. Considering a 14 kPa CO_2 and 6 kPa H_2O binary mixture and fixing the adsorption and desorption temperature at 400 K and 300 K respectively, it is possible to examine $\alpha(\Delta H,400\text{ K})$–$\alpha(\Delta H,300\text{ K})$ and check the correspondence of the simulations with the theoretical model.

Fig. 11 shows the difference between the CO_2/H_2O selectivity at 400 K and 300 K as taken from the binary simulations. It is expressed as a function of the difference in adsorption enthalpy between CO_2 and H_2O assessed with single-component *NVT* simulations. The IZA frameworks are color coded according to their CO_2/N_2 selectivity at 400 K (determined using IAST), to ensure that despite the high temperature, the framework is still selective enough for CO_2 with respect to N_2. The blue line corresponds to the theoretical Langmuir model that was derived previously (Fig. 4b). Materials which are explicitly mentioned in the text are indicated in both Fig. 11 and subsequent plots.

The shape of the theoretical curve qualitatively follows the simulation data points. First of all, at negative values for $\Delta H_{CO_2} - \Delta H_{H_2O}$, there is a deep trench of points for which the CO_2/H_2O selectivity is lower at 400 K than at 300 K. The corresponding frameworks are therefore not suited for the HALD process, although they show very favorable CO_2/N_2 selectivities (20 and up). Secondly, for enthalpy differences between 0 and 10 kJ mol^{-1}, there is a group of materials (including MFI) that perform better than most other materials and also have high CO_2/N_2 selectivities. Finally, for values higher than 10 kJ mol^{-1}, there is a long tail of materials that show decreasing performance with increasing ΔH. In this region, most CO_2/N_2 selectivities are also low. The discrepancy between the simulation data and the theoretical curve is most likely due to the larger number of adsorption sites for H_2O than for CO_2, partly driven by the formation of H_2O networks.

In conclusion, the difference in adsorption enthalpy between CO_2 and H_2O as determined by *NVT* simulations provides a first indication of candidate materials that are suited for the concept of high-temperature adsorption & low-temperature desorption and this could simplify the search in further screening procedures. In the next section, we will determine what materials have the best performance among the materials that show HALD behavior.

6 Selection of the best materials

Before selecting the best performing materials, it is necessary to determine which criteria are the most important. Bae and Snurr proposed five criteria to evaluate the performance of nanoporous materials for CCS: CO_2 uptake, CO_2/N_2 selectivity, CO_2 working capacity, regenerability and a sorbent selection parameter.[58] Some of these parameters can be translated into the context of HALD.

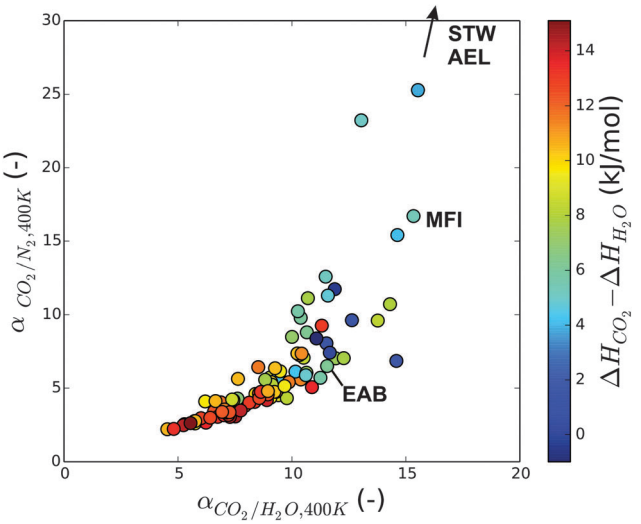

Fig. 12 CO_2/N_2 *versus* CO_2/H_2O selectivity at 400 K, color coded with the difference in adsorption enthalpy between CO_2 and H_2O.

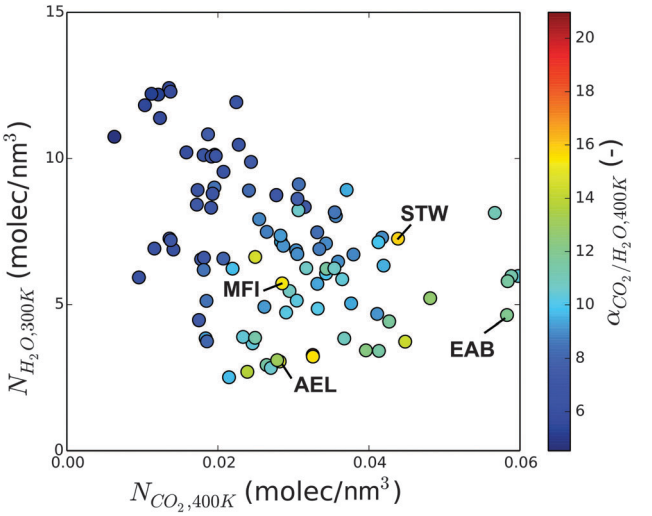

Fig. 13 H_2O uptake at 300 K *versus* CO_2 uptake at 400 K, color coded with the CO_2/H_2O selectivity.

As we discussed earlier, the CO_2/H_2O selectivity at 400 K is of paramount importance, because it is the basis of the competitive adsorption behavior. It is also important the CO_2/N_2 selectivity does not drop at high temperature. In Fig. 12, the CO_2/N_2 *versus* CO_2/H_2O selectivity at 400 K shows a high correlation. Materials that show good selectivity for CO_2 at high temperature, do so both when competing with H_2O and with N_2. The color code in Fig. 12 further demonstrates that the materials with the lowest $\Delta H_{CO_2} - \Delta H_{H_2O}$ have the highest selectivities. Materials that do not show HALD behavior have not been included, so the range of ΔH is smaller than in Fig. 11. This further highlights the sensitivity of the HALD method: ΔH should be low, but if it is too low, the material does not show the HALD behavior anymore.

Apart from the CO_2/H_2O and CO_2/N_2 selectivity, the amount of adsorbed CO_2 is important as well. As the adsorption takes place at high temperature, only small amounts of CO_2 are adsorbed. To minimize the size of the adsorption column, it is desirable to maximize the CO_2 uptake of the material at high temperature. Note that in this competitive adsorption, the CO_2 uptake and working capacity are in principle the same: if enough pure H_2O is added to the material in the regeneration cycle, H_2O will completely substitute the CO_2 that is present in the material. This is not the case for conventional carbon capture, where even at high temperature or low pressure, some residual CO_2 may be left in the material.

Finally, the amount of H_2O that is necessary to regenerate the material through competitive adsorption at low temperature is also important. Fig. 13 shows that there is no clear correlation between the H_2O uptake at 300 K (desorption conditions) and the CO_2 uptake at 400 K (adsorption conditions). The H_2O working capacity is the difference between the loading at 300 K and 100 kPa pure H_2O and the H_2O loading at 400 K and the 6 kPa H_2O/14 kPa CO_2 binary mixtures, but since the latter term is negligible compared to the first term, the H_2O working capacity is approximately equal to the uptake at 300 K. In Fig. 13, we are therefore interested in materials with a high CO_2 uptake at 400 K and a low H_2O uptake at 300 K. The CO_2 uptake at 400 K is two orders of magnitude lower than the H_2O uptake at 300 K. To put this in perspective however, for the binary CO_2/H_2O mixtures, the H_2O loading drops by more than 3 orders of magnitude between 300 K and 400 K, whereas the CO_2 loading drops only by one. This is exactly the competitive advantage of CO_2 adsorption at high temperature.

To find the material with an optimal combination of all mentioned properties, a multicriteria optimization is necessary. Lejaeghere *et al.* reported how promising materials, with various competing properties, can be selected from a database with a post-Pareto algorithm.[40] From all data points, a so-called Pareto set is determined *i.e.* a selection of the materials that no other candidate can improve on with respect to all criteria simultaneously. Then, a minimum win fraction is defined, which represents the trade-off between the different Pareto solutions: how much minimally needs to be sacrificed of one set of properties to improve some other properties, while also considering relative importances of the properties. Below, we will apply this approach to the four previously mentioned properties of HALD.

In Table 1, the criteria and their units are reported. The uptake is defined as the volumetric uptake in molecules per nm^3, to emphasize the volume of the adsorption column, rather than the weight. The third column shows the relative importance of the criteria, the last column the objective of the optimization (maximization or minimization). The weighing of the criteria is performed by normalizing each property to its

Table 1 Properties optimized with the Pareto approach, the units, their relative weights and the objective (to maximize or to minimize the criterion)

Property	Unit	Weight	Objective
α_{CO_2/H_2O}	(—)	1	Max
α_{CO_2/N_2}	(—)	1	Max
$N_{CO_2,400K}$	molecules per nm^3	1	Max
$N_{H_2O,300K}$	molecules per nm^3	1	Min

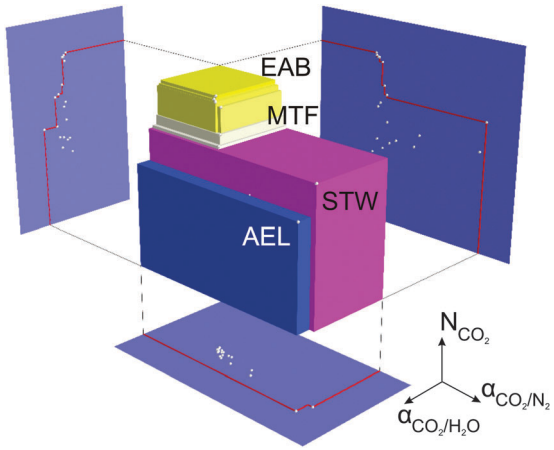

Fig. 14 Graphical representation of the Pareto set (a so-called skyline plot), *i.e.* the selection of materials that outperform each other material with respect to at least one property. Results for the CO_2/H_2O selectivity, the CO_2/N_2 selectivity and the CO_2 uptake are depicted. The H_2O uptake has been omitted from this plot, but is considered in the overall analysis. The planes represent 2D projections of the 3D plot.

range in the entire zeolite data set, followed by a multiplication by the appropriate scaling factor. Here, all criteria are considered equally important. In the ESI,† we show that increasing the importance of the CO_2/H_2O and CO_2/N_2 selectivity does not have a large influence on the obtained minimum win fractions.

Fig. 14 graphically shows the Pareto front for three out of four criteria. The H_2O uptake is omitted in this 3D graphical representation, but is taken into account in the minimum win fractions. In Table 2, the minimum win fractions of these materials are given. The AEL framework surfaces as the best material: with respect to STW, AEL has a slightly lower CO_2/N_2 selectivity and smaller CO_2 uptake, but this is compensated by a better CO_2/H_2O selectivity and smaller H_2O uptake. EAB has one of the highest CO_2 uptakes, but performs worse for the other criteria. MFI is not a part of the Pareto set, although it is clear from Fig. 12 and 13 that its performance is relatively close to the best performing materials.

The Pareto set does not change drastically when the adsorption temperature is set to 375 K, 350 K or 325 K (a Pareto analysis at these temperatures is included in the ESI†) and also the relative order of the materials in the set remains more or less unchanged. The AEL framework outperforms the other materials for all temperatures considered. The advantage of adsorption temperatures that are not as high as 400 K, is the higher CO_2 uptake at that temperature. For AEL for instance, CO_2 uptake is only 0.03 molecules per nm^3 at 400 K, but rises to 0.20 molecules per nm^3 at 325 K, while keeping the competitive advantage over H_2O. By optimizing the adsorption temperature, the efficiency of HALD can therefore be increased.

Pareto analyses are gaining attention for engineering applications[59,60] but are still brand new in the field of carbon capture. By using this innovative post-Pareto approach, we have highlighted some potential candidates for HALD behavior, based on multiple criteria. The method is transferrable to larger screenings[10] and other materials.[61]

Table 2 Minimum win fractions (mwf) showing the optimality of the materials in the Pareto set, with respect to the CO_2/H_2O selectivity, CO_2/N_2 selectivity and CO_2 uptake at 400 K of the binary mixture and the H_2O uptake at 300 K and 100 kPa

mwf (−) (%)		mwf (−) (%)	
AEL	57.4	VET	3.2
STW	42.6	PAU	2.9
EAB	29.9	TER	2.9
MTF	19.4	CAN	2.1
STI	17.7	RTE	2.1
AWW	16.9	ATO	1.9
UFI	9.9	MTT	1.4
LTF	9.5	TON	1.3
LEV	8.7	AFO	0.5
IHW	7.5		

7 Perspectives and conclusions

The concept of high-temperature adsorption & low-temperature desorption (HALD) provides potentially major advantages over conventional technologies. Most importantly, there is in principle no energy penalty on the CO_2/N_2 separation, as HALD effectively uses the waste heat of the exhaust gases to regenerate the nanoporous material. Additionally, H_2O in the flue gas is no longer sabotaging CCS due to the competitive advantage of CO_2 in the adsorption cycle.

First of all, a breakdown of the Gibbs free adsorption energy of CO_2 and H_2O shows that if $\Delta H_{ads,H_2O} < \Delta H_{ads,CO_2} < 0$ and $\Delta S_{ads,H_2O} < \Delta S_{ads,CO_2} < 0$, H_2O adsorbs preferentially at low temperature, but at a high enough temperature, CO_2 adsorption will become more favorable. This is confirmed by a simple Langmuir model, which expresses the CO_2/H_2O selectivity as a function of $\Delta H_{CO_2} - \Delta H_{H_2O}$ (a material property) and the temperature (a process condition), *i.e.* $\alpha(\Delta H,T)$.

Grand Canonical Monte Carlo simulations for the commercially available all-silica MFI can be used to investigate the HALD concept in more detail. In this case, the adsorption enthalpy for CO_2 and H_2O is fixed, so the CO_2/H_2O selectivity is only dependent on the temperature, $\alpha(T)$. Adsorption at 400 K favors the adsorption of CO_2 over H_2O, although the loading of both components is very low. Desorption of CO_2 is obtained by saturation of the framework with pure H_2O at 300 K. Optimizing the adsorption and desorption conditions might provide room for improvements in both selectivity and uptake. This example already shows the challenges that may arise when deploying HALD on an industrial scale. The working capacity of any nanoporous material at high temperatures is low and therefore, large adsorption columns may be required. Moreover, since the H_2O loading at 300 K is much higher than the CO_2 loading at 400 K, large amounts of H_2O will be needed for the regeneration of the material. However, it might be beneficial to perform the adsorption at temperatures that are somewhat lower than 400 K, to have a reasonable CO_2 loading, as well as a competitive advantage.

Furthermore, the Langmuir model can also rationalize the results of a screening of the IZA database. Across the materials

in this database, ΔH_{CO_2} and ΔH_{H_2O} change, but if we fix the process conditions (partial pressures and temperatures), it is possible to evaluate $\alpha(\Delta H)$. Not only is this an excellent validation of the model, it also demonstrates that the CO_2/H_2O selectivity can be predicted solely with single-component adsorption enthalpies, that are computationally much easier to assess, providing an interesting perspective for future studies. There is an enormous database of existing and even commercial nanoporous materials that could be suitable for the HALD process and screenings based on molecular simulations have proven to be successful in the past.[14,31] Such a screening also allows to compare the performance of different materials for HALD.

To determine the best performing materials, we argue that the most important parameters of the HALD method are the CO_2/H_2O selectivity, CO_2/N_2 selectivity, the CO_2 uptake at high temperature and H_2O uptake at low temperature. An innovative Pareto-based search algorithm can identify the most promising materials for HALD (including AEL, STW, EAB and MTF), considering the four criteria simultaneously.

Finally, the results in this manuscript do not only intend to provide a proof of principle for the HALD method, they are highly relevant to the conventional operation of carbon capture with nanoporous materials as well. Industrial flue gases always contain some H_2O, which will compete with CO_2 for adsorption sites in the pores of the material. We showed that a small increase in the adsorption temperature might already shift this competition in favor of CO_2, thereby reducing the H_2O uptake in the adsorption step and lowering the regeneration cost of the material. Moreover, in the conventional regeneration cycle, heating of the material is sometimes done by injecting steam directly into the adsorption bed. Also here, the competition of H_2O with CO_2 is a very important factor, as the competitive advantage of CO_2 over H_2O at high temperature may actually reduce the efficiency of this steam injection approach.

In conclusion, the upside-down HALD alternative to traditional CCS methods opens new perspectives to reduce the energy penalty of CCS, to validate the waste heat of the exhaust gases in the CO_2/N_2 separation and to overcome competitive adsorption of H_2O.

Acknowledgements

L.J., K.L. and V.V.S. acknowledge the Fund for Scientific Research – Flanders (FWO), the Research Board of Ghent University (BOF) and BELSPO in the frame of IAP/7/05 for financial support. L.J. is a 2013–2014 grantee of the Commission for Educational Exchange between the United States and Belgium, which administers the Fulbright Belgium and Fulbright Schuman programs. V. V. S. acknowledges funding from the European Research Council under the European Community's Seventh Framework Programme (FP7(2007–2013) ERC grant agreement number 240483). J.M.H. was supported by the Deutsche Forschungsgemeinschaft (DFG, priority program SPP 1570). B.S. was supported as part of the Center for Gas Separations Relevant to Clean Energy Technologies, an Energy Frontier Research Center funded by the U.S. Department of Energy, Office of Science, Office of Basic Energy Sciences under Award Number DE-SC0001015. We thank Wim De Witte for help with Fig. 1 and 2. L.J. thanks Steven Vandenbrande for fruitful discussions.

References

1 B. Smit, J. R. Reimer, C. M. Oldenburg and I. C. Bourg, *Introduction to Carbon Capture and Sequestration*, Imperial College Press, London, 1st edn, 2014.
2 J. Wilcox, *Carbon Capture*, Springer, New York, 1st edn, 2012.
3 S. Pacala and R. Socolow, *Science*, 2004, **305**, 968–972.
4 V. Scott, S. Gilfillan, N. Markusson, H. Chalmers and R. S. Haszeldine, *Nat. Clim. Change*, 2013, **3**, 105–111.
5 R. M. Bethea, *Air Pollution Control Technology*, John Wiley & Sons, New York, 1978.
6 G. T. Rochelle, *Science*, 2009, **325**, 1652–1654.
7 G. Rochelle, E. Chen, S. Freeman, D. Van Wagener, Q. Xu and A. Voice, *Chem. Eng. J.*, 2011, **171**, 725–733.
8 D. M. D'Alessandro, B. Smit and J. R. Long, *Angew. Chem., Int. Ed.*, 2010, **49**, 6058–6082.
9 S. Choi, J. Drese and C. Jones, *ChemSusChem*, 2009, **2**, 796–854.
10 M. W. Deem, R. Pophale, P. A. Cheeseman and D. J. Earl, *J. Phys. Chem. C*, 2009, **113**, 21353–21360.
11 M. M. F. Hasan, E. L. First and C. A. Floudas, *Phys. Chem. Chem. Phys.*, 2013, **15**, 17601–17618.
12 T.-H. Bae, M. R. Hudson, J. A. Mason, W. L. Queen, J. J. Dutton, K. Sumida, K. J. Micklash, S. S. Kaye, C. M. Brown and J. R. Long, *Energy Environ. Sci.*, 2013, **6**, 128–138.
13 J. Kim, M. Abouelnasr, L.-C. Lin and B. Smit, *J. Am. Chem. Soc.*, 2013, **135**, 7545–7552.
14 A. O. Yazaydin, R. Q. Snurr, T.-H. Park, K. Koh, J. Liu, M. D. LeVan, A. I. Benin, P. Jakubczak, M. Lanuza, D. B. Galloway, J. J. Low and R. R. Willis, *J. Am. Chem. Soc.*, 2009, **131**, 18198–18199.
15 M. Fernandez, P. G. Boyd, T. D. Daff, M. Z. Aghaji and T. K. Woo, *J. Phys. Chem. Lett.*, 2014, **5**, 3056–3060.
16 N. T. T. Nguyen, H. Furukawa, F. Gnndara, H. T. Nguyen, K. E. Cordova and O. M. Yaghi, *Angew. Chem., Int. Ed.*, 2014, 10645–10648.
17 B. Wang, A. P. Cote, H. Furukawa, M. O'Keeffe and O. M. Yaghi, *Nature*, 2008, **453**, 207–211.
18 D. Yuan, W. Lu, D. Zhao and H.-C. Zhou, *Adv. Mater.*, 2011, **23**, 3723–3725.
19 W. Lu, D. Yuan, D. Zhao, C. I. Schilling, O. Plietzsch, T. Muller, S. Bräse, J. Guenther, J. Blümel, R. Krishna, Z. Li and H.-C. Zhou, *Chem. Mater.*, 2010, **22**, 5964–5972.
20 M. E. Davis and R. F. Lobo, *Chem. Mater.*, 1992, **4**, 756–768.
21 C. Baerlocher and L. McCusker, Database of Zeolite Structures, 2014, http://www.iza-structure.org/databases.
22 E. Flanigen, J. Bennett, R. Grose, J. Cohen, R. Patton, R. Kirchner and J. Smith, *Nature*, 1978, **271**, 512–516.

23 M. Schenk, S. L. Vidal, T. J. H. Vlugt, B. Smit and R. Krishna, *Langmuir*, 2001, **17**, 1558–1570.
24 S. Calero, B. Smit and R. Krishna, *Phys. Chem. Chem. Phys.*, 2001, **3**, 4390–4398.
25 Y. Oumi, A. Miyajima, J. Miyamoto and T. Sano, Impact of Zeolites and other Porous Materials on the new Technologies at the Beginning of the New Millennium, Proceedings of the 2nd International FEZA (Federation of the European Zeolite Associations) Conference, Elsevier, 2002, vol. 142, pp. 1595–1602.
26 P. Bai, M. Tsapatsis and J. I. Siepmann, *Langmuir*, 2012, **28**, 15566–15576.
27 N. Desbiens, A. Boutin and I. Demachy, *J. Phys. Chem. B*, 2005, **109**, 24071–24076.
28 M. Trzpit, M. Soulard, J. Patarin, N. Desbiens, F. Cailliez, A. Boutin, I. Demachy and A. H. Fuchs, *Langmuir*, 2007, **23**, 10131–10139.
29 T. Sano, H. Yanagishita, Y. Kiyozumi, F. Mizukami and K. Haraya, *J. Membr. Sci.*, 1994, **95**, 221–228.
30 T. J. H. Vlugt and M. Schenk, *J. Phys. Chem. B*, 2002, **106**, 12757–12763.
31 L.-C. Lin, A. H. Berger, R. L. Martin, J. Kim, J. A. Swisher, K. Jariwala, C. H. Rycroft, A. S. Bhown, M. Deem, M. Haranczyk and B. Smit, *Nat. Mater.*, 2012, **11**, 633–641.
32 J. M. Huck, L.-C. Lin, A. Berger, M. N. Shahrak, R. L. Martin, A. Bhown, M. Haranczyk, K. Reuter and B. Smit, *Energy Environ. Sci.*, 2014, 4132–4146.
33 McKinsey&Company, *Carbon Capture & Storage: Assessing the Economics*, 2008, http://www.globalccsinstitute.com/publications/carbon-capture-storage-assessing-economics.
34 S. Heylen, S. Smeekens, C. Kirschhock, T. Parac-Vogt and J. A. Martens, *Energy Environ. Sci.*, 2010, **3**, 910–916.
35 S. Heylen, L. Joos, T. N. Parac-Vogt, V. Van Speybroeck, C. E. A. Kirschhock and J. A. Martens, *Angew. Chem., Int. Ed.*, 2012, **51**, 11010–11013.
36 S. Sircar, *Ind. Eng. Chem. Res.*, 2006, **45**, 5435–5448.
37 L. Grajciar, J. Cejka, A. Zukal, C. Otero Arean, G. Turnes Palomino and P. Nachtigall, *ChemSusChem*, 2012, **5**, 2011–2022.
38 R. Krishna, B. Smit and S. Calero, *Chem. Soc. Rev.*, 2002, **31**, 185–194.
39 J. F. M. Denayer, R. A. Ocakoglu, I. C. Arik, C. E. A. Kirschhock, J. A. Martens and G. V. Baron, *Angew. Chem., Int. Ed.*, 2005, **44**, 400–403.
40 K. Lejaeghere, S. Cottenier and V. Van Speybroeck, *Phys. Rev. Lett.*, 2013, **111**, 075501.
41 V. Pareto, *Manuale di economia politica con una introduzione alla scienza sociale*, Società Editrice Libraria, Milano, 1906.
42 Department of Energy – National Energy Technology Laboratory, *Cost and Performance Baseline for Fossil Energy Plants*, 2013, http://www.netl.doe.gov/research/energy-analysis/energy-baseline-studies.
43 D. Dubbeldam, A. Torres-Knoop and K. S. Walton, *Mol. Simul.*, 2013, **39**, 1253–1292.
44 D. Frenkel and B. Smit, *Understanding Molecular Simulation: From Algorithms to Applications*, Academic Press, San Diego, 2nd edn, 2002.
45 B. Smit and T. L. M. Maesen, *Chem. Rev.*, 2008, **108**, 4125–4184.
46 A. J. O'Malley and C. R. A. Catlow, *Phys. Chem. Chem. Phys.*, 2013, **15**, 19024–19030.
47 A. L. Myers and J. M. Prausnitz, *AIChE J.*, 1965, **11**, 121–127.
48 D. W. Hand, S. Loper, M. Ari and J. C. Crittenden, *Environ. Sci. Technol.*, 1985, **19**, 1037–1043.
49 A. García-Sánchez, C. O. Ania, J. B. Parra, D. Dubbeldam, T. J. H. Vlugt, R. Krishna and S. Calero, *J. Phys. Chem. C*, 2009, **113**, 8814–8820.
50 H. J. C. Berendsen, J. R. Grigera and T. P. Straatsma, *J. Phys. Chem.*, 1987, **91**, 6269–6271.
51 L. Joos, J. A. Swisher and B. Smit, *Langmuir*, 2013, **29**, 15936–15942.
52 M. Pinheiro, R. L. Martin, C. H. Rycroft, A. Jones, E. Iglesia and M. Haranczyk, *J. Mol. Graphics Modell.*, 2013, **44**, 208–219.
53 R. L. Martin, B. Smit and M. Haranczyk, *J. Chem. Inf. Model.*, 2012, **52**, 308–318.
54 R. L. Martin, T. F. Willems, L.-C. Lin, J. Kim, J. A. Swisher, B. Smit and M. Haranczyk, *ChemPhysChem*, 2012, **13**, 3595–3597.
55 J. Castillo, D. Dubbeldam, T. Vlugt, B. Smit and S. Calero, *Mol. Simul.*, 2009, **35**, 1067–1076.
56 A. Goj, D. S. Sholl, E. D. Akten and D. Kohen, *J. Phys. Chem. B*, 2002, **106**, 8367–8375.
57 J. M. Castillo, J. Silvestre-Albero, F. Rodriguez-Reinoso, T. J. H. Vlugt and S. Calero, *Phys. Chem. Chem. Phys.*, 2013, **15**, 17374–17382.
58 Y.-S. Bae and R. Q. Snurr, *Angew. Chem., Int. Ed.*, 2011, **50**, 11586–11596.
59 N. Assadian and S. H. Pourtakdoust, *Adv. Space Res.*, 2010, **45**, 398–409.
60 S. Liu, R. Tao and C. M. Tam, *Habitat Int.*, 2013, **37**, 155–162.
61 C. E. Wilmer, M. Leaf, C. Y. Lee, O. K. Farha, B. G. Hauser, J. T. Hupp and R. Q. Snurr, *Nat. Chem.*, 2012, **4**, 83–89.